International Journal of Extreme Manufacturing

Grain refining in weld metal using short-pulsed laser ablation during CW laser welding of 2024-T3 aluminum alloy

OPEN ACCESS
IOP Publishing | IMMT
International Journal of Extreme Manufacturing
Int. J. Extrem. Manuf. 1 (2019) 045003 (8pp)
https://doi.org/10.1088/2631-7990/ab563a

Grain refining in weld metal using short-pulsed laser ablation during CW laser welding of 2024-T3 aluminum alloy

Masaki Kasuga, Tomokazu Sano and Akio Hirose

Division of Materials and Manufacturing Science, Graduate School of Engineering, Osaka University, 2-1 Yamada-oka, Suita, Osaka 565-0871, Japan

E-mail: sano@mapse.eng.osaka-u.ac.jp

Received 28 September 2019, revised 6 November 2019
Accepted for publication 11 November 2019
Published 3 December 2019

Abstract

The 2024 aluminum alloy is used extensively in the aircraft and aerospace industries because of its excellent mechanical properties. However, the weldability of 2024 aluminum alloy is generally low because it contains a high number of solutes, such as copper (Cu), magnesium (Mg), and manganese (Mn), causing solidification cracking. If high speed welding of 2024 aluminum alloy without the use of filler is achieved, the applicability of 2024 aluminum alloys will expand. Grain refining is one of the methods used to prevent solidification cracking in weld metal, although it has never been achieved for high-speed laser welding of 2024 aluminum alloy without filler. Here, we propose a short-pulsed, laser-induced, grain-refining method during continuous wave laser welding without filler. Bead-on-plate welding was performed on a 2024-T3 aluminum alloy at a welding speed of 1 m min^{-1} with a single mode fiber laser at a wavelength of 1070 nm and power of 1 kW. Areas in and around the molten pool were irradiated with nanosecond laser pulses at a wavelength of 1064 nm, pulse width of 10 ns, and pulse energy of 430 mJ. The grain-refinement effect was confirmed when laser pulses were irradiated on the molten pool. The grain-refinement region was formed in a semicircular shape along the solid–liquid interface. Results of the vertical section indicate that the grain-refinement region reached a depth of 1 mm along the solid–liquid interface. The Vickers hardness test results demonstrated that the hardness increased as a result of grain refinement and that the progress of solidification cracking was suppressed in the grain refinement region.

Keywords: 2024 aluminum alloy, hot cracking, laser welding, grain refinement, dendrite fragmentation, short pulsed laser, laser ablation

(Some figures may appear in colour only in the online journal)

1. Introduction

Aluminum alloys are widely used for products, such as aircraft and automobiles, due to their excellent specific strength, corrosion resistance, and processability [1–3]. From a manufacturing perspective, high-speed and high-quality laser welding is required to shorten production time, delivery lead time, and cost. Aluminum has a large linear expansion coefficient, so a low melting point solidification phase is generated when laser welding an aluminum alloy due to solidification cracking [4, 5]. Grain refinement has been used as a material strengthening method because it reduces solidification cracking [6] and improves mechanical properties, such as ductility and strength [7, 8]. In general, coarsening of the weld grain and segregation of a low melting point alloy phase occurs after an alloy is welded and solidified, which leads to degradation of mechanical properties and deterioration of chemical properties, such as

corrosion resistance [6]. If the grains of the solidified metal could be refined, the low melting point alloy phase could be dispersed and the concentration of the strain released, resulting in a significant improvement in the resistance to solidification cracking.

A number of grain-refining methods have been studied [9–14] to improve solidification crack resistance, such as adding grain refiner with filler, [9, 10] applying an external magnetic field parallel to the welding electrode [11], imposing ultrasonic vibration on the surface of the base material [12], applying ultrasonic vibration directly to the molten pool via an inserted tungsten probe [13], and the arc oscillation method [14]. Crushing and melting of primary crystal dendrites [15], formation of a partial supercooling region by induced pressure [16], and improvement of the wettability of impurities occur [17] as a result of the aforementioned treatments. In these research studies, it was reported that the susceptibility to solidification cracking is lowered because the formation of equiaxed crystal formation is promoted [9–17]. However, there are several drawbacks to current grain-refining methods that include dimension limitations for ultrasonic vibration, difficulty in following high-speed laser welding while in contact with a high temperature molten pool, and adding inoculant by feeding fillers.

The generation of noncontact, high-strength stress waves that follow laser welding can be achieved by irradiating with a high-intensity pulsed laser, which generates the recoil force of the ablation plasma expansion and propagates a pressure wave inside the solid/liquid. A number of studies regarding laser shock generation have been conducted since the 1980 s [18–21], e.g. 10 GPa is generated when an Nd:YAG laser with a pulse width of 3 ns at a wavelength of 1064 nm is used to irradiate aluminum in a vacuum [18, 21]. Here, we propose a short-pulsed, laser-induced, grain-refining method, which is a new welding method that irradiates a high-intensity, short-pulsed laser around the weld pool during continuous wave (CW) laser welding. By using a short-pulsed laser, we can apply a stress wave to the solid–liquid interface for grain refining while avoiding the drawbacks of current methods.

Applying the short-pulsed, laser-induced, grain-refining method to an aluminum alloy has the potential to achieve high-speed and high-quality welding without solidification cracking in aluminum. However, the effect of short-pulsed laser irradiation during CW laser welding on the grain refinement of aluminum alloy weld metal has never been reported. The purpose of this study was to investigate the influence of short-pulsed laser irradiation position on a weld metal structure by irradiating a short-pulsed laser during laser welding.

2. Experimental methods

A 2024-T3 aluminum alloy with a thickness of 3.175 mm was used. The chemical composition of this alloy is shown in table 1. Acetone was used to remove oil and moisture before laser welding. Bead-on-plate laser welding was performed in the direction perpendicular to the rolling direction. A schematic of the experimental setup for laser welding is shown in figure 1. Welding experiments were carried out using a single-mode fiber laser (Furukawa Electric Co., Ltd, FEC1000S) with a wavelength of 1070 nm and a power of 1000 W at a welding speed of 16.6 mm s^{-1}.

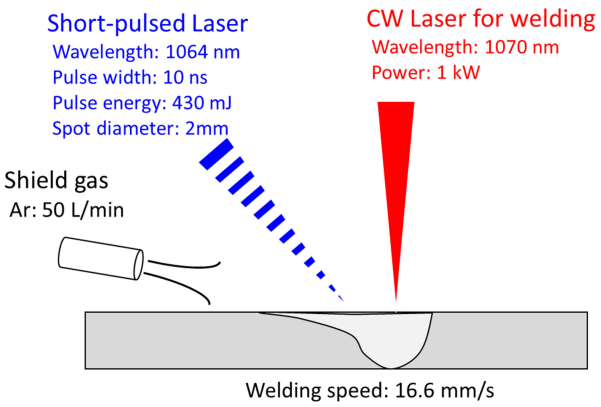

Figure 1. Experimental setup for laser welding.

Table 1. Chemical composition of 2024-T3 (thickness: 3.175 mm) (mass%).

Si	Fe	Cu	Mn	Mg	Cr	Zn	Ti	Al
0.05	0.16	4.6	0.64	1.5	0.00	0.09	0.03	Bal.

In order to evaluate the influence of the short-pulsed laser irradiation position on the solidified structure, the relative position between the welding laser irradiation position and the short-pulsed laser irradiation position was altered. The short-pulsed laser irradiation position was changed to the front, rear, boundary, and side of the molten pool. For this experiment, a Nd:YAG laser (Spectra-Physics, Quanta-Ray®) with a pulse width of 10 ns, a wavelength of 1064 nm, a pulse energy of 430 mJ, and a frequency of 10 Hz was used. Laser pulses ware focused to a spot size of 2.1 mm using a plano-convex lens with a focal length of 2 m, corresponding to an intensity of 1.3×10^9 W cm^{-2}. The positions of short-pulsed laser irradiation are shown in figure 2. In this paper, the irradiation position is expressed using (x, y) coordinates, e.g. $(x, y) = (1.5, 0)$. As shown in figure 2, the welding direction was described using the positive x-axis; and the vertical direction was described using the y-axis. The shape of the molten pool and spot diameter were measured with a high-speed camera.

In situ observation using a high-speed camera (NAC Image Technology Inc., MEMRECAM HX-3) was carried out, and the effect of short-pulsed laser irradiation on molten pool flow was observed. In this observation, 10 000 frames s^{-1} was used, and an additional laser (JENOPTIK Optical Systems GmbH, JOLD-45-CPXF-IL) with a wavelength of 938 ± 5 nm combined with a narrow band pass filter with a central wavelength of 940 ± 10 nm in front of the camera was used for illumination.

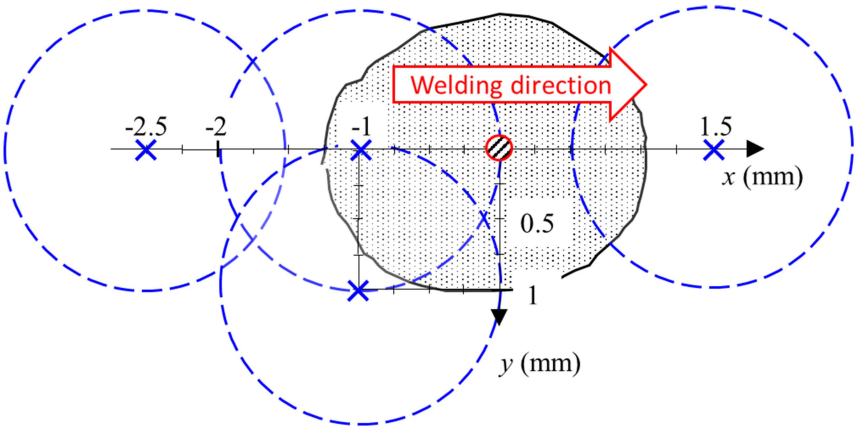

Position of CW laser irradiation
Shape of molten pool of A2024-T3 welded at 16.6 mm/s
Area of short-pulsed laser irradiation
Spot center of short-pulsed laser

Coordinate (x,y) of spot center of short-pulsed laser (unit: mm)	Position	Comment
(1.5,0)	Front	Partially inside
(-2.5,0)	Rear	Completely outside
(-1,1)	Side	Partially inside
(-1,0)	Boundary	Mostly inside

Figure 2. Positions of laser irradiation.

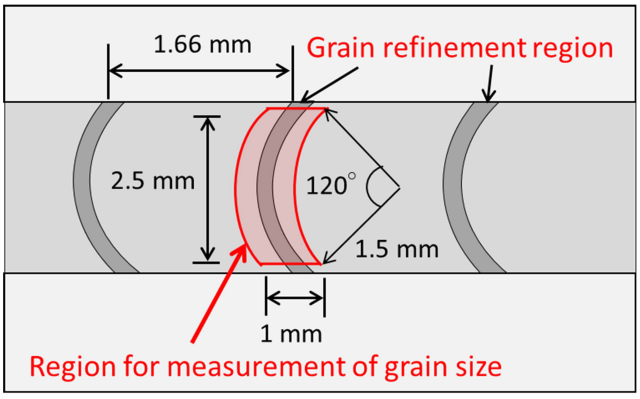

Figure 3. Grain size measurement region.

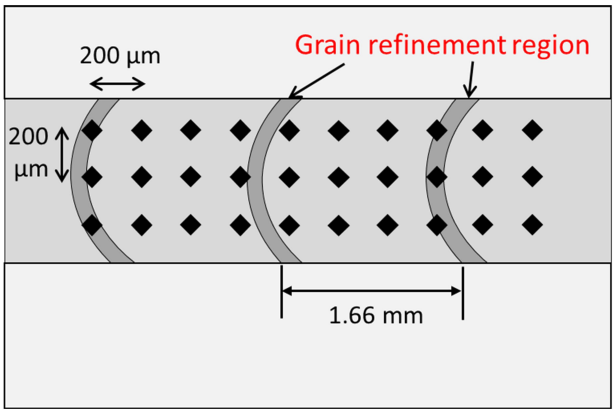

Figure 4. Schematic of measured positions for the hardness test.

The specimen for microstructure observation was removed from the position 15 mm away from the joining starting end. The specimen was subjected to mirror polishing by buffing and to anodic electrolytic etching with Barker's reagent for 3 min at a voltage of 20 V. The etched samples were then analyzed using a polarization microscope.

Measurement of average grain size was performed on the test piece under each irradiation condition by the Jeffries method, and the influence of the short-pulsed laser on the grain size was evaluated. In the Jeffries method, the grain size is calculated by measuring the grain number Na within the target area A. The number of grains located on the boundary line of the target area is counted as $1/2$. The average grain size, $d = \sqrt{A/Na}$, was determined from A and Na. In order to evaluate the short-pulsed laser affected region, measurements were performed in the region, as shown in figure 3, on each test piece.

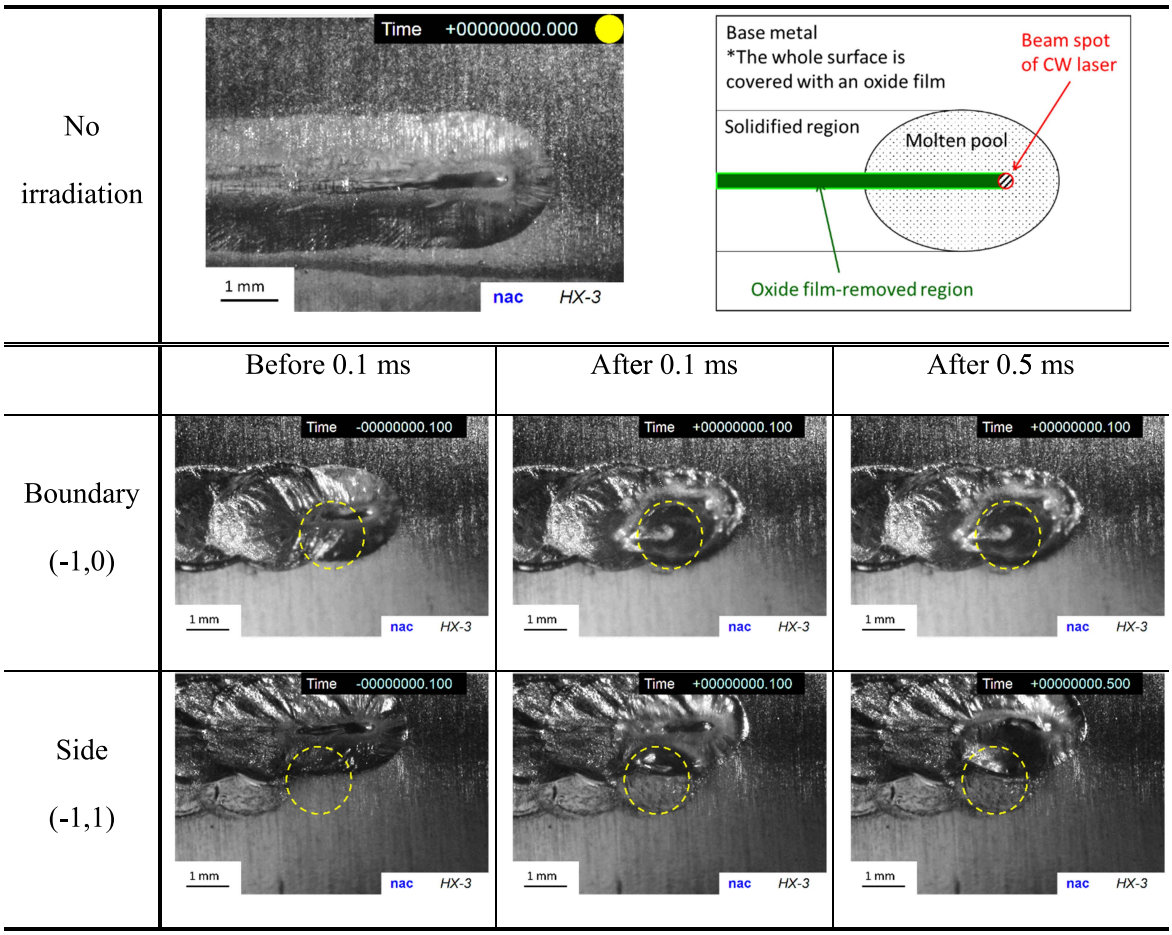

Figure 5. High-speed photographs of 2024-T3 aluminum alloy irradiated at various positions. Yellow dashed circles indicate short-pulsed laser irradiation area.

The Vickers hardness test was carried out on the specimen irradiated with the short-pulsed laser at $(x, y) = (-1, 0)$, which demonstrated the most grain refinement; and the influence of the grain refinement on the hardness was measured. The hardness test was performed on the area along the bead center at a load of 1.96 N and a holding time of 10 s at a measurement interval of 200 μm. The measurement position is shown in figure 4.

3. Results

3.1. Observation of molten pool during short-pulsed laser irradiation using a high-speed camera

High-speed camera images of the weld pool surface during short-pulsed laser irradiation are shown in figure 5. The time at which the ablation plasma was confirmed on the surface is defined as $T = 0$. Since the pulse width was 10 ns and the plasma emission time was not observed over two frames (0.2 ms), the temporal error of the definition of $T = 0$ is considered to be within 0.1 ms. When only laser welding was performed, we observed that the oxide film melted only at the location directly irradiated with the laser and remained in the form of a film on the surface of the molten pool. This

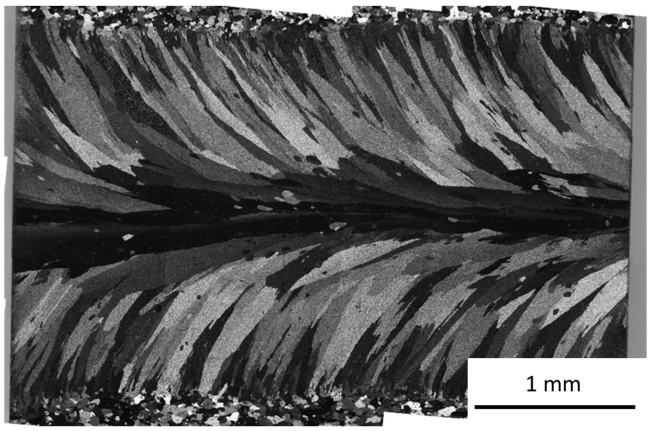

Figure 6. Polarized optical microscope image of 2024-T3 aluminum alloy without short-pulsed laser irradiation.

occurred because the melting point of aluminum oxide (2072 °C) is higher than that of pure aluminum (660 °C) [1].

When short-pulsed laser irradiation was directly applied to the inside of the molten pool $(x, y) = (-1, 0)$, the entire molten pool was significantly deformed by the ablation pressure. When irradiating partially inside the molten pool $(x, y) = (-1, 1)$, we observed that the wave front propagated from the side of the melt pool 1 mm away from the weld line.

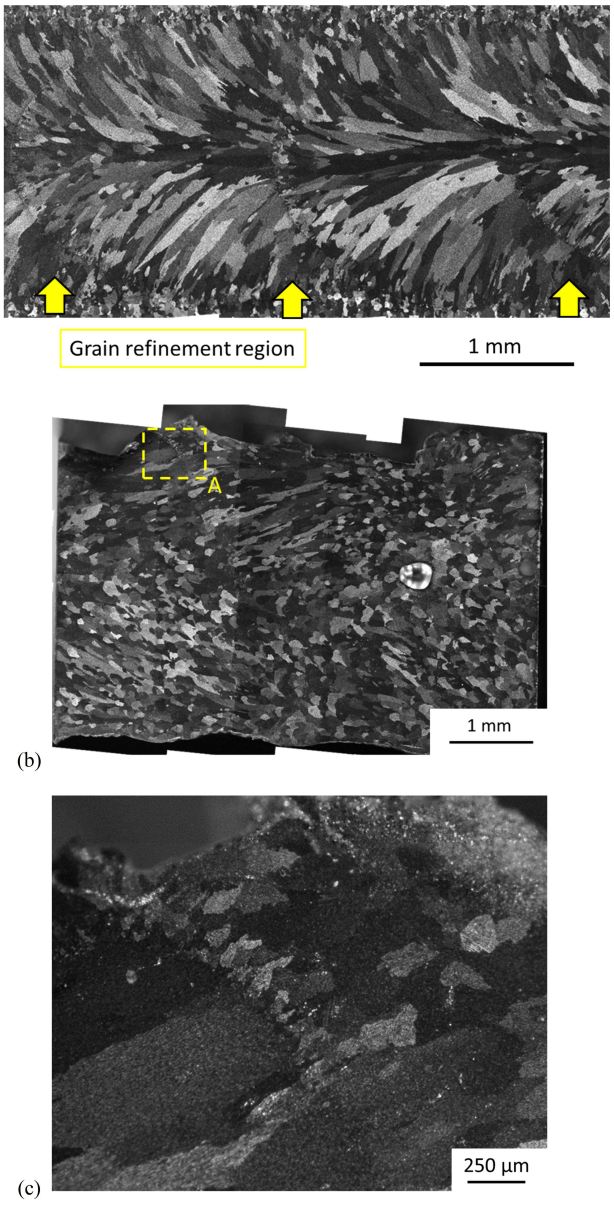

Figure 7. Polarized optical microscope image of 2024-T3 aluminum alloy irradiated by short-pulsed laser at boundary $(x, y) = (-1, 0)$. Micrographs show the: (a) front surface, (b) vertical cross-section, and (c) magnified image of region A in (b).

In all conditions, the short-pulsed laser irradiated the surface oxide film, not the molten aluminum.

3.2. Grain structure in weld metal

Micrographs of the surface and vertical sections in the weld metal using a polarizing microscope are shown in figures 6–8. The welding direction in each image is from the left to the right of the image. As shown in figure 6, analysis of the grain structure when only laser welding was performed at a welding speed of $16.6\,\mathrm{mm\,s^{-1}}$ demonstrates that the weld metal structure was composed mainly of columnar crystals epitaxially grown from the base material and stray crystals, with few equiaxed crystals formed.

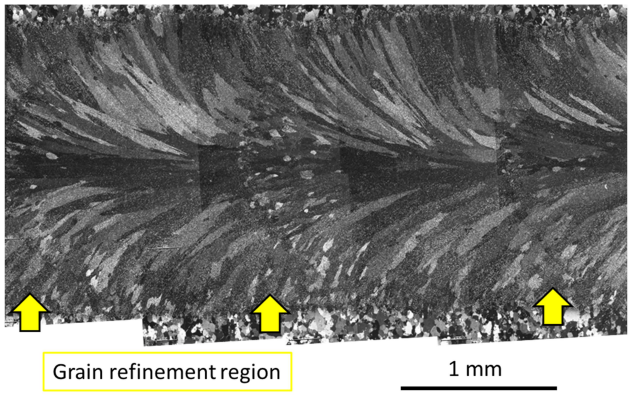

Figure 8. Polarized optical microscope image of 2024-T3 aluminum alloy irradiated by short-pulsed laser at side $(x, y) = (-1, 1)$.

The micrographs in figure 7(a) show the grain structure of the specimen irradiated primarily with the short-pulsed laser in the molten pool $(x, y) = (-1, 0)$. The grain-refined region was periodically formed in a semicircular shape due to the bead surface. Figure 7(b) shows the vertical section; and figure 7(c) shows the enlargement of region A, as indicated in figure 7(b). The grain-refined region existed in a row at a depth of approximately 1 mm, as can be seen in figure 7(c).

Figure 8 shows the observation results of the specimen irradiated partially inside the molten pool $(x, y) = (-1, 1)$. The grain-refined region was also periodically formed in a semicircular shape. As shown in figures 7 and 8, the interval between grain refinement regions was 1.66 mm. Since the welding speed is $16.6\,\mathrm{mm\,s^{-1}}$ and the repetition rate of the short-pulsed laser is 10 Hz, the spatial interval of the pulses is 1.66 mm/pulse, which corresponds to the interval between grain refinement regions. Therefore, these grain refinement regions are due to the pulsed laser irradiation. Although the short-pulsed laser was irradiated to a part of the molten pool, the refined region of the crystal grain was semicircular. This indicates that the short-pulsed laser was effective on the solid–liquid interface where the short-pulsed laser was not directly irradiated.

3.3. Grain size

The number of crystal grains under each laser irradiation condition was measured, and the mean crystal grain size, shown in figure 9, was calculated. This graph shows that the average grain size decreased when the pulse laser was irradiated, and the average grain size significantly decreased when the pulse laser was irradiated at a boundary of 1 mm behind the welding laser. However, when the short-pulsed laser was irradiated at the front and rear of the welding laser, the grain refinement effect was small. The measurement region for the number of crystal grains includes a region that is not grain refined, so the strict average crystal grain size of the grain refinement region became smaller. For example, in figure 7(a), the grain size of a fine crystal grain was approximately 30 μm.

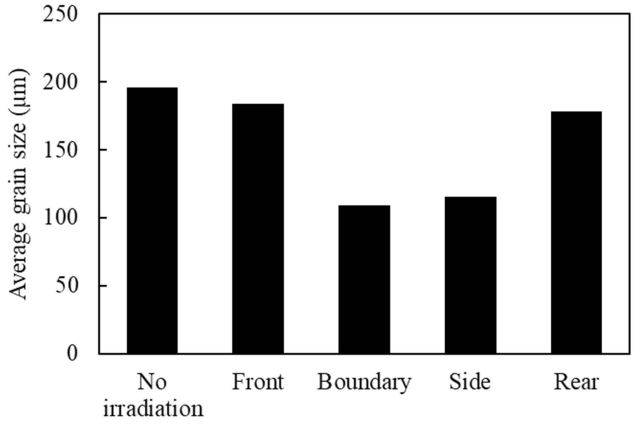

Figure 9. The average grain size for each irradiation position.

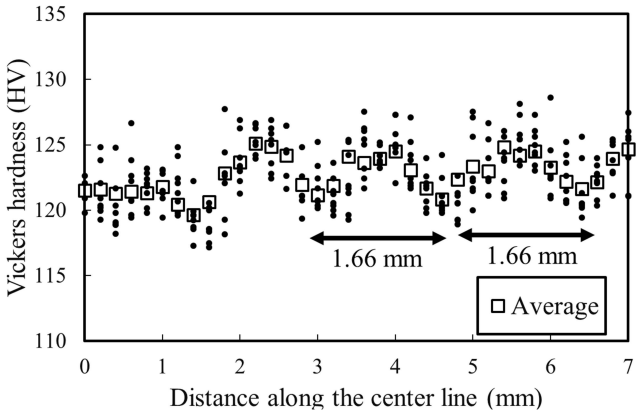

Figure 10. Hardness distribution of longitudinal direction on surface irradiated at boundary $(x, y) = (-1, 0)$.

3.4. Hardness

Figure 10 shows the results of Vickers hardness tests on the weld metal of specimens irradiated with a short-pulsed laser at boundary $(x, y) = (-1, 0)$ during laser welding. The average hardness of the base metal was 120 HV. This graph shows that the hardness periodically increased and decreased along the weld line. Since this period was approximately 1.66 mm intervals, it suggests that the increase in hardness was due to grain-refining by the short-pulsed laser irradiation. This graph indicates that grain refinement by irradiating pulse laser can increase the Vickers hardness by approximately 5 HV.

3.5. Suppression of solidification crack growth

Figure 11 shows micrographs of the specimen irradiated with a short-pulsed laser into the weld pool $(x, y) = (-1, 0)$ under welding conditions where weld solidification cracking occurs. These images show that the progress of solidification cracking was suppressed in the grain refinement region. This was because grain refinement results in the dispersion of the low melting point alloy phase and relaxation of stress concentration. This result indicates that the short-pulsed, laser-induced grain-refining method has the potential to suppress solidification cracking for high-speed laser welding without adding grain refiner.

4. Discussion

Figure 7 shows that the grain refinement region was generated at the solid–liquid interface at a depth of 1 mm and a width of 300 μm. Based on experimental results, we proposed that the grain refinement was caused by two mechanisms: dendrite fragmentation and dynamic nucleation.

4.1. Dendrite fragmentation

As illustrated in figure 12, the factors influencing dendrite fragmentation were stress wave propagation and forced convection, which affected the solid–liquid interface. These factors were due to the recoil force of the ablation plasma generated on the surface. While the molten metal convection affected the solid–liquid interface by propagating matter and heat, stress waves propagated only pressure.

Since ultrahigh-pressure states can be generated, fundamental research on pressure waves propagating substances by short-pulsed laser has been actively conducted since the 1980s [18–21]. Here, we used the Phipps model, which has been used in experiments conducted on aluminum without using a plasma confinement medium [18, 21]. Internal bubbles, reflected stress waves, and temperature gradients inside the molten pool are not addressed in this paper. Since there was a solid oxide coating on the surface, we assume that the absorptance of the laser was similar to solid aluminum.

Phipps *et al* conducted a short-pulsed laser irradiation experiment in which the laser intensity (I, W cm^{-2}), wavelength (λ, μm), and pulse width (τ, ns) were varied over a wide range in a vacuum. The empirical trend of the ablation pressure was expressed by [18, 21]

$$P_a/I = b(I\lambda\sqrt{\tau})^n, \tag{1}$$

where P_a is the ablation pressure (Mbar), and the constant b depends on the material ($b = 5.6$ and $n = -0.3 \pm 0.03$ for aluminum). This empirical equation was established in the ranges of 3–70 TW cm^{-2} for laser intensity, 1.5 ms–500 ps for pulse width, and 10.6 μm–248 nm for wavelength.

The applied pulse force product, ζ, is estimated by

$$\zeta = P_a\tau \text{ (Mbar ns)} = 3.39 \times 10^{-3} \times I^{0.7} \times \lambda^{-0.3} \times \tau^{0.85}. \tag{2}$$

The irradiation conditions of the short-pulsed laser were substituted into this equation, and the maximum ablation pressure was obtained as follows:

$$P_a = 3.93 \times 10^{-1} \times I^{0.7} \times \lambda^{-0.3} \times \tau^{-0.75} = 0.328 \text{ GPa}. \tag{3}$$

Thus, the ablation pressure in the Phipps model was estimated to be 0.328 GPa.

The strength of a dendrite at high temperature was evaluated [22] using a model in which a single rod placed in a fluid breaks by flow. According to Frost and Ashby [23], the

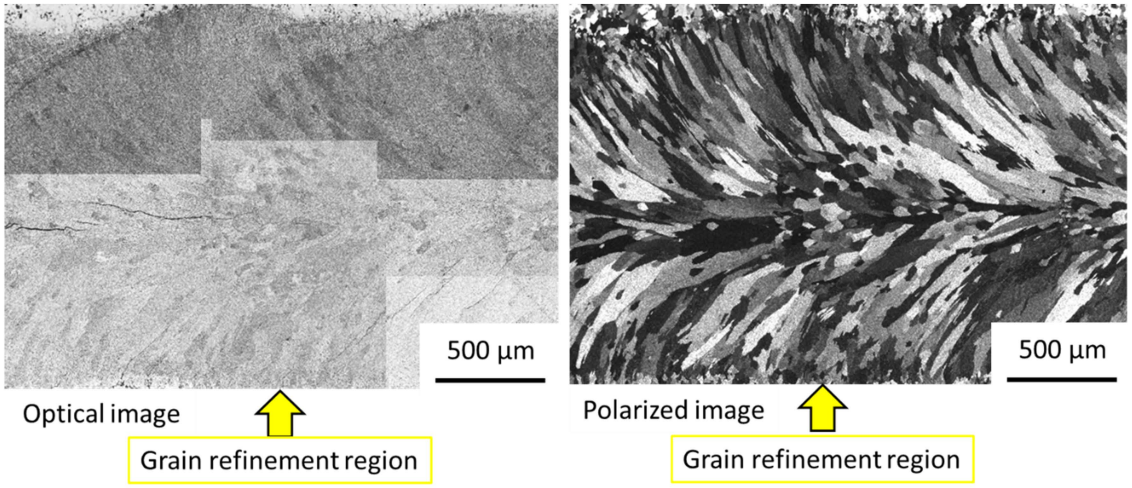

Figure 11. Observation of crack end irradiated at boundary $(x, y) = (-1, 0)$.

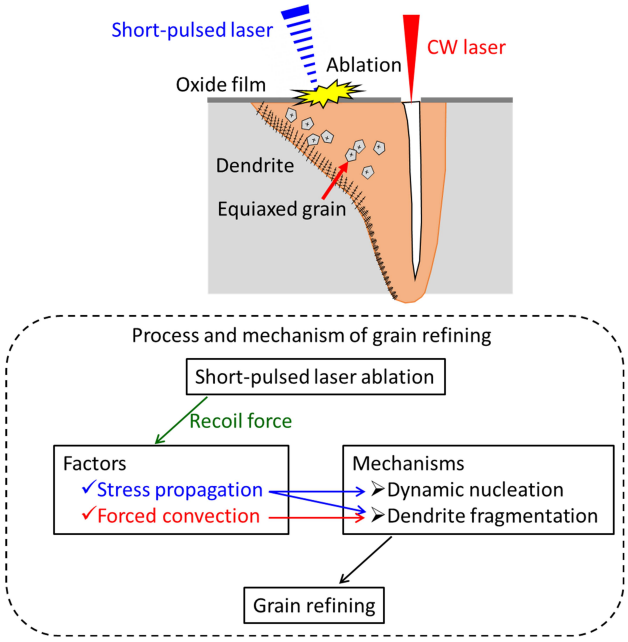

Figure 12. Schematic of the process and mechanism of grain refining.

yield stress of solidified metal at the temperature near the melting point is expressed by the following equations:

$$\sigma_y = 10^{-3} \cdot E(T), \tag{4}$$

$$E(T) = E_{300}\left[1 + B\left(\frac{T - 300}{T_m}\right)\right], \tag{5}$$

where σ_y (MPa) is the yield stress, $E(T)$ (GPa) is the Young's modulus at absolute temperature T, E_{300} is the Young's modulus (70 GPa) at 300 K, T_m is the melting point (933 K), and B is −1.33 (for aluminum) [24]. The yield stress at the melting point was estimated to be 6.8 MPa, which was smaller than the stress wave of 328 MPa estimated using the Phipps model, indicating that the dendrite was deformed and broken.

Dendrite breakage was likely due to molten metal convection as the grain-refining region was 1 mm deep from the surface. Crushed dendrites flowing into the molten pool became nuclei and formed fine equiaxed crystals.

4.2. Dynamic nucleation

This dynamic nucleation caused by the driving force from the short-pulsed laser, ablation-induced pressure wave can be explained by the following two concepts [10, 25]. Generally, impurity particles, such as oxides, carbides, nitrides, and borides, were mixed in the molten metal during the casting and welding processes. It is hypothesized that pressure improves the wettability of impurities in the molten pool, enabling impurity particles to act as heterogeneous nuclei [10].

Alternatively, the temporary solidification temperature change, dT/dp, occurs due to the increase in pressure; and thus, heterogeneous nucleation occurs due to an increase in undercooling degree as the melting point rises [25]. This is indicated by the Clapeyron equation

$$\frac{dT}{dp} = T_E \frac{(V_L - V_S)}{L}, \tag{6}$$

where V_L and V_s are the volume of the liquid and the solid, respectively, at the equilibrium solidification temperature T_E; and L is the latent heat of solidification. The volume change accompanying solidification is included through the term $(V_L - V_S)$. The Clapeyron equation indicates that the solidification temperature of a volume-shrinking metal during solidification increases with increasing pressure. When high pressure is applied to a liquid cooled to near the nucleation temperature, the solidification temperature rises and rapidly becomes undercooled, then heterogeneous nuclei, such as impurities, work effectively; and the grain structure is refined [17].

The experimental result that the grain-refined region concentrates at the solid–liquid interface is in agreement with the explanation that the undercooling degree increases near the solidification temperature. The pressure wave generated by the short-pulsed laser ablation improves the wettability of

impurities and promotes heterogeneous nucleation, which is considered one miniaturization mechanism.

5. Conclusions

Grain refinement in 2024 aluminum alloy weld metal was achieved by short-pulsed laser ablation during laser welding, where the progress of solidification cracking was suppressed. The Vickers hardness test results showed that the hardness increased due to the effects of grain refinement. We propose that the increase of the equiaxial crystal formation sites due to dendrite crushing was one of the grain-refinement mechanisms because the pressure wave generated by the short-pulsed laser exceeded dendrite strength in a high temperature state. Based on the experimental results, we suppose that grain refinement is induced by two mechanisms: dendrite fragmentation and dynamic nucleation.

This method has the potential to suppress solidification cracking for high-speed laser welding without adding grain refiner. Improving solidification structure of an aluminum alloy weld by using this method will enable highly reliable high-speed laser welding and expand the range of applications for aluminum alloys.

Acknowledgments

The authors would like to thank Mr Tetsuji Kuwabara of NAC Image Technology Inc. for support of high-speed photographing. This work was supported in part by MEXT Quantum Leap Flagship Program (MEXT Q-LEAP) Grant No. JPMXS0118068348, JSPS KAKENHI Grant Nos. JP16H04247, JP16K14417, and 19K22061. This work was funded in part by ImPACT Program of Council for Science, Technology and Innovation (Cabinet Office, Government of Japan).

ORCID iDs

Tomokazu Sano https://orcid.org/0000-0003-2624-5092

References

[1] Totten G E and Mackenzie D S 2003 *Handbook of Aluminum* (Boca Raton, FL: CRC Press)
[2] Dursun T and Soutis C 2014 *Mater. Des.* **56** 862
[3] Cole G S and Sherman A M 1995 *Mater. Charact.* **35** 3
[4] Ion J C 2000 *Sci. Technol. Weld. Joining* **5** 265
[5] Hagenlocher C, Weller D, Weber R and Graf T 2019 *Sci. Technol. Weld. Joining* **24** 313
[6] Davies G J and Garland J G 1975 *Int. Metall. Rev.* **196** 83
[7] Petersen W A 1973 *Weld. Res. Suppl.* **53** 74
[8] Hall E O 1951 *Proc. Phys. Soc.* B **64** 747
[9] Mohanty P S and Gruzleski J E 1995 *Acta Metall.* **43** 2001
[10] Eskin G I and Eskin D G 2014 *Ultrasonic Treatment of Light Alloy Melts* (Boca Raton, FL: CRC Press)
[11] Pearce B P and Kerr H W 1981 *Metall. Trans.* B **12B** 479
[12] Chen Q-H, Lin S-B, Yang C-L, Fan C-L and Ge H-L 2016 *Acta Metall. Sin.* **29** 1081
[13] Tao Y, Sindo K and Zhen L 2016 *Acta Mater.* **106** 144
[14] Tao Y, Zhen L and Sindo K 2016 *Acta Mater.* **116** 166
[15] Wang S, Kang J, Guo Z, Lee T L, Zhang X, Wang Q, Deng C and Mi J 2019 *Acta Mater.* **165** 388
[16] Hunt J D and Jackson K A 1966 *J. Appl. Phys.* **37** 254
[17] Ramirez A, Qian M, Davis B, Wilks T and John D St 2008 *Scr. Mater.* **59** 19
[18] Fabbro R, Fournier J, Ballard P, Devaux D and Virmont J 1990 *J. Appl. Phys.* **68** 775
[19] Davies S J, Edward C, Taylor G S and Palmer S B 1993 *J. Phys. D: Appl. Phys.* **26** 329
[20] Fairand B P and Clauer A H 1979 *J. Appl. Phys.* **50** 1497
[21] Phipps C R, Turner T P, Harrison R F, York G W, Osborne W Z, Anderson G K, Corlis X F, Haynes L C, Steele H S and Spicochi K C 1988 *J. Appl. Phys.* **64** 1083
[22] Pilling J and Hellawell A 1996 *Metall. Mater. Trans.* **27A** 229
[23] Frost H J and Ashby M F 1982 *Deformation Mechanism Maps: The Plasticity and Creep of Metals and Ceramics* (Oxford: Oxford University Press)
[24] Pilling J and Ridley N 1986 *Acta Metall.* **34** 669
[25] Hunt J D and Jackson K A 1966 *J. Appl. Phys.* **37** 254